

Some nonlinear interactive effects in bubbly clouds

By SANJAY KUMAR† AND CHRISTOPHER E. BRENNEN

California Institute of Technology, Pasadena, CA 91125, USA

(Received 2 January 1992 and in revised form 11 August 1992)

Nonlinear interactive effects in a bubbly cloud have been studied by investigating the frequency response of a bubble layer bounded by a wall oscillating normal to itself. Averaged equations of motion are used and the Rayleigh–Plesset equation is used to include the bubble dynamics. Energy dissipation due to viscous and thermal effects are included while relative motion between the two phases, liquid compressibility and viscous dissipation in the liquid have been ignored. First, a Fourier analysis of the Rayleigh–Plesset equation is used to obtain an approximate solution for the nonlinear response of a single bubble in an infinite fluid. This is used in an approximate calculation of the nonlinear frequency response of a bubble layer. Finite thickness of the bubble layer results in characteristic natural frequencies of the layer all of which are less than the natural frequency of a single bubble. The presence of bubbles of different sizes in the layer causes a phenomenon called *harmonic cascading*. This phenomenon consists of a large response at twice the excitation frequency when the mixture contains bubbles with a natural frequency equal to twice the excitation frequency. The details of these results along with most important limitations of theory are presented.

1. Introduction

The purpose of this research is to gain some understanding of the global effects of bubble dynamics in the fluid mechanics of bubbly flows. At the most basic level, bubble–bubble interactions occur because the pressure changes generate rapid bubble volume changes which cause accelerating velocity fields which effect the pressure distribution in the flow. Such an interaction in a layer of gaseous bubbles is considered in the present work. These gaseous bubbles may be generated by the collapse of vaporous bubbles in cavitating flows and may determine the final phase of noise emission in such flows occurring in ship propellers, hydrofoils and turbomachines. Understanding of such flows is also important for acoustical techniques of flow measurement. Also, gas bubble oscillations precede the development of vaporous cavitation and the results from present work are aimed at an understanding of this stage.

Traditionally, bubble flows have been studied using single-bubble dynamics and assuming no interaction among the bubbles in the flow field. Such an approach ignores the interactive effects that the bubble dynamics have on the global pressure distribution in the flow field and is accurate only in the case of extremely dilute bubble concentrations. The experimental results of Arakeri & Shanmuganathan (1985) have shown that noise produced by travelling bubble cavitation can be modified by interactive effects at higher bubble concentrations. Marboe, Billet & Thompson (1986)

† Present address: Room 2-336, Massachusetts Institute of Technology, Cambridge, MA 02139, USA.

measured noise spectra in travelling bubble cavitation and observed lower frequencies than can be explained on the basis of single-bubble theories. Both papers indicate interactive effects occurring for flows with large concentrations of bubbles. To model these effects researchers have used continuum models incorporating bubble dynamics to analyse interactive effects. d'Agostino & Brennen (1988) and Omta (1987) found that the characteristic natural frequencies of a spherical cloud of bubbles can be much smaller than the natural frequency of a single bubble. However, these recent analyses use linearized models of the bubble dynamics and the flow. It is well known that the dynamics of a bubble can be quite nonlinear (Prosperetti 1974, 1975) which in combination with nonlinear convective effects may produce significant nonlinear effects in bubbly flows. The objective of the present research is to understand these nonlinear effects by studying an analytically amenable model problem.

The nonlinear dynamics in the growth and collapse of a single bubble have been studied for a long time (e.g. Plesset & Prosperetti 1977). Early studies, based on space-averaged equations, did not include bubble dynamic effects, but treated the bubbly mixture as an equivalent compressible homogeneous medium (Tangren, Dodge & Seifert 1949). Among the first to focus on the dynamics of bubble clusters was van Wijngaarden (1964) who analysed the collapse of a large number of bubbles next to a flat wall and found considerable increase in the pressure at the wall as a result of the interactive effects. Biesheuvel & van Wijngaarden (1984) used ensemble and volume averaging of the conservation equations for each phase to develop more general equivalent flow models of dispersed two-phase mixtures, including the phenomena of bubble dynamics, relative motion and liquid compressibility. Most of the subsequent research efforts are based on these equations.

Mørch (1980, 1982) considered the collapse of a spherical bubble cloud assuming that the pressure increase would lead to shock formation at the cloud boundary and that the shock would propagate inward and completely annihilate bubbles in its path. This model did not include individual bubble dynamics and predicted infinite pressure and infinite collapse velocities as the radius approached zero. In a subsequent paper Hansson, Kedrinskii & Mørch (1982) constructed a model using a continuum mechanics approach and used the Rayleigh–Plesset equation to model the bubble dynamics. Chahine (1982) developed a method using matched asymptotic expansions. This model assumes instantaneous transmission of ambient conditions to the bubbles and thus neglects the compressibility of the bubble cloud. It was found that because of interactive effects in the cloud, the larger the number of bubbles in the cloud, the more delayed and violent is the implosion and thus larger pressures are generated. The method is limited to low-void-fraction flows and to a small number of bubbles in a specified configuration. Chahine (1983) also developed a model using a continuum mechanics approach and first-order gradient theory. Recently Omta (1987) has obtained analytical solutions for small-amplitude oscillations and numerical solutions for large amplitudes. Omta linearized the Biesheuvel–van Wijngaarden (1984) equations and obtained solutions under a number of simplifying assumptions. The bubble cloud was found to possess characteristic natural frequencies which depended upon the void fraction with the lowest characteristic natural frequency dominating the cloud behaviour. d'Agostino & Brennen (1988) also solved for the linearized dynamics of spherical bubble clouds using a continuum mechanism model with bubble dynamics under more general conditions. This model includes various dissipative mechanisms including the relative motion between phases. The conclusions were found to be essentially the same as those of Omta (1987). d'Agostino, Brennen & Acosta (1988) also solved for the linearized dynamics of the flow of bubbly mixture over slender surfaces.

Recently Birnir & Smereka (1990) have carried out numerical solutions for bubble clouds and investigated the solutions using the techniques used to study dynamical systems. They found that the bubble radius, the flow velocity and pressure were bounded and the cloud was seen to possess natural frequencies. Periodic solutions were found to be stable for weak excitation. It is clear that much remains to be learnt about the highly nonlinear dynamics of bubbles and bubble clouds.

The objective of present work is to develop a methodology for handling nonlinear terms and to obtain nonlinear solutions by studying the dynamics of a bubbly liquid next to a flat wall which oscillates normal to its own plane. The case of a layer of identical bubbles has been examined. Also, a semi-infinite layer with a given bubble size distribution has been examined and reveals the new phenomena of *harmonic cascading* in such clouds. The purpose is to obtain a qualitative understanding of the various mechanisms of frequency dispersion in the bubbly two-phase mixtures.

2. Some typical applications and values

Clouds of gas bubbles occur in a variety of technological situations. These are generated by collapsing bubbles in vaporous cavitation (Blake, Wolpert & Geib 1977; Ceccio & Brennen 1991) and the dynamics of these clouds of small gas bubbles are clearly important. Gas bubble oscillations may precede onset of vaporous cloud cavitation as bubbles acquire critical size through equilibrium oscillation growth (Mørch 1989). Though the process of rectified diffusion for such a growth is not included in the present model, the present analysis can be applied to bubble clouds at timescales finer than that required for bubble growth through rectified gaseous diffusion. The typical data used for illustration of the present analysis have been selected with these physical situations in mind.

A number of researchers have measured the size of free-stream nuclei (Gates & Acosta 1978) and cavitation bubbles (Maeda, Yamaguchi & Kato 1991). Typical nuclei range in size from 10 to 150 μm ; the size distribution can usually be approximated by

$$\eta(R_0) = N^*/R_0^m, \quad (1)$$

where $\eta(R_0)dR_0$ is the number of nuclei per unit liquid volume (in m^{-3}) with equilibrium radii between R_0 and $R_0 + dR_0$ (in m). A distribution of the form given by (1) has been used to describe the size distribution of free-stream nuclei in sea water and various water tunnel facilities with $N \approx 10^{-5} \text{m}^{-\frac{1}{2}}$ and $m \approx 3.5$ (Brennen & Ceccio 1989). The bubble size distribution in cavitation clouds (Maeda *et al.* 1991) can also be approximately described by (1) with suitable values of N^* and m .

The void fraction values due to free-stream nuclei are extremely small. Though the void fraction of a cavitation cloud is larger than that of free stream, it is still small at approximately 0.03% (Maeda *et al.* 1991). No measurements of the void fraction of a cloud resulting from the breakup of a collapsing cavitation bubble exist. For the purpose of illustrating the present results, void fractions were estimated from the experiments of Arakeri & Shanmuganathan (1985). Table 1 presents two sets of typical data obtained by these means. The fluid has been chosen to be water at room temperature (20 °C). A bubble subject to periodic excitation oscillates with a value of the polytropic constant, k , between 1 and γ (Plesset & Hsieh 1960) and so, for illustrative purposes, the value of the polytropic constant, k , has been chosen to be 1. The values in the water tunnel set are typical of cavitation nuclei in a water tunnel where the static pressure has been lowered. Similarly, the values in the ocean set represent conditions in flows near the ocean surface at atmospheric conditions. When

Application	R_0 (μm)	$P_{\infty 0}$ (Pa)	k	$\nu/\omega_b R_0^2$	$S/\rho\omega_b^2 R_0^3$	$10^{-5} \omega_b$ (rad/s)
Water tunnel	14	13 146	1	0.01	0.10	5.2
Ocean	20	101 325	1	0.0028	0.012	8.8

TABLE 1. Fluid and bubble parameters for the examples presented. These data are for water at 20 °C.

a distribution of bubble sizes is used, the form given by (1) will be employed and a continuum of bubble sizes between 10 and 100 μm will be used.

The present work is aimed at small-amplitude oscillation of gas bubbles. It is well known that bubbles which grow to a size larger than a critical size grow into vaporous bubbles and collapse violently. This threshold growth is given by (Flynn 1964, p. 88)

$$[R/R_0]_{cr} = (7.48 P_{g0}/P_{\infty 0})^{1/3}, \quad (2)$$

where R_0 is the equilibrium bubble radius, P_{g0} the permanent gas pressure in the bubble and $P_{\infty 0}$ the far-field pressure at the equilibrium condition. Considering the values given in table 1, a bubble must grow to 4.6 times its equilibrium size for the water tunnel conditions and 7.1 times its equilibrium size for the ocean conditions before it grows explosively and then collapses violently like a vaporous bubble. Clearly, the small-amplitude oscillations at less than 100% change in the bubble size, presented here, are well within the gas bubble region.

3. Nonlinear solution for a single bubble

There exists a substantial body of literature on the nonlinear dynamics of a single bubble in an infinite fluid (Plesset & Prosperetti 1977). In the present context it is appropriate to note that Eller & Flynn (1969) solved the problem of subharmonics of order one-half using a perturbation procedure and that Prosperetti (1974, 1975) generated nonlinear analytical solutions for subharmonics and harmonics of various orders using a perturbation method. Parlitz *et al.* (1990) have studied extensively the dynamics of a single bubble. In the present work it is necessary to construct the very simplest nonlinear solution of the Rayleigh–Plesset equation for a single bubble. Later this will be used as a building block for the problem of many bubbles interacting in a flow. The bubble is assumed to be spherical and to contain water vapour and residual permanent gas. The bubble interior is assumed to be uniform with constant vapour pressure, P_v . The permanent gas in the bubble is assumed to behave polytropically with an index, k , between 1 and γ (Plesset & Hsieh 1960). The liquid compressibility is only included in the radiation damping and this is done by including it in the effective viscosity used for the bubble dynamics (Devin 1959; Prosperetti 1977). Bubble growth due to rectified diffusion has been ignored since that takes place on a much slower timescale than the natural cycle of the bubble (Hsieh & Plesset 1961). With these assumptions the Rayleigh–Plesset equation describing the bubble dynamics becomes

$$R \frac{D^2 R}{Dt^2} + \frac{3}{2} \left(\frac{DR}{Dt} \right)^2 + \frac{4\nu DR}{R Dt} + \frac{2S}{\rho R} = \frac{P_v - P_{\infty}(t)}{\rho} + \frac{P_{g0}}{\rho} \left(\frac{R_0}{R} \right)^{3k}. \quad (3)$$

In the present solution a Fourier series expansion is used and terms up to second order are retained in order to examine the corrections to the linear solution. The bubble radius, $R(t)$, and the pressure at infinity, $P_{\infty}(t)$, are expanded in the form

$$R = R_0 + \sum_{n=1}^N \operatorname{Re}(R_n e^{in\delta t}), \tag{4}$$

$$\frac{P_\infty(t)}{\rho} = P_0 + \sum_{n=1}^N \operatorname{Re}(P_n e^{in\delta t}), \tag{5}$$

where $P_0 = P_{\infty 0}/\rho$ with $P_{\infty 0}$ being far-field equilibrium pressure in the liquid; P_n and R_n are complex quantities, and the frequencies $n\delta$, $n = 1, N$ represent a discretization of the frequency domain. These expansions are substituted into (3) and all terms of third or higher order in R_n/R_0 are neglected in order to extract the simplest nonlinear effects. Finally, coefficients of $e^{in\delta t}$ on both sides of the simplified equation are equated to yield the following relation for P_n and R_n :

$$\frac{P_n}{\omega_b^2 R_0^2} = \Lambda(n) \frac{R_n}{R_0} + \sum_{j=1}^{n-1} \beta_1(n, j) \frac{R_j}{R_0} \frac{R_{n-j}}{R_0} + \sum_{j=1}^{N-n} \beta_2(n, j) \frac{\bar{R}_j}{R_0} \frac{R_{n+j}}{R_0}, \tag{6}$$

where the overbar denotes complex conjugate and the bubble natural frequency, ω_b is given by

$$\omega_b = \left(\frac{3kP_{g0}}{\rho R_0^2} - \frac{2S}{\rho R_0^3} \right)^{\frac{1}{2}} \tag{7}$$

and $\Lambda(n)$, $\beta_1(n, j)$ and $\beta_2(n, j)$ are defined as

$$\Lambda(n) = \left[\frac{n^2 \delta^2}{\omega_b^2} - 1 - i \frac{n\delta}{\omega_b} \frac{4\nu}{\omega_b R_0^2} \right], \tag{8}$$

$$\beta_1(n, j) = \frac{3k+1}{4} + \frac{3k-1}{2} \frac{S}{\rho \omega_b^2 R_0^3} + \frac{1}{2} \frac{\delta^2}{\omega_b^2} (n-j) \left(n + \frac{j}{2} \right) + i \frac{2\nu}{\omega_b R_0^2} \frac{\delta}{\omega_b} (n-j), \tag{9}$$

and
$$\beta_2(n, j) = \frac{3k+1}{2} + (3k-1) \frac{S}{\rho \omega_b^2 R_0^3} + \frac{1}{2} \frac{\delta^2}{\omega_b^2} (n^2 - nj - j^2) + i \frac{2\nu}{\omega_b R_0^2} \frac{n\delta}{\omega_b}. \tag{10}$$

Using a Newton–Raphson scheme, (6) is solved iteratively for R_n/R_0 given P_n , the fluid properties and individual bubble characteristics. It was seen numerically that if there is a single excitation frequency, ω_f , then the only non-zero components of the bubble oscillation, R_n , will occur at harmonics of that single excitation frequency. It is also seen that the response R_n/R_0 decays with increase in the order of the harmonic and is negligible (amplitude $\ll 10^{-20}$) at harmonics of order higher than 50. Thus calculating the response up to 50 harmonics was considered sufficient. It is also clear from (9) and (10) that $\beta_1(n, j)$ and $\beta_2(n, j)$ are functions of $n\delta/\omega_b$ and j/n . Furthermore, note from (6) that for a single excitation frequency, the only coefficients $\beta_1(n, j)$ and $\beta_2(n, j)$ that enter the calculations are those for which j and n take values corresponding to harmonics of the excitation frequency. Consequently the only values of $n\delta/\omega_b$ and j/n which enter the calculations are those which are ratios of an excitation frequency harmonic to the natural frequency of the bubble or two excitation frequency harmonics. Hence, despite the explicit appearance of δ , the results of the calculation are independent of this parameter used in discretizing the frequency domain. Finally, note also that the pressure perturbation coefficients, P_n , occur in (6) only in linear form and thus can be large without introducing error into the solution. However, the analysis is valid only for $|R_n/R_0| \ll 1$. This defines the extent of the weak nonlinear effects which are examined here and indirectly implies an upper limit on the magnitude of $P_n/\omega_b^2 R_0^2$.

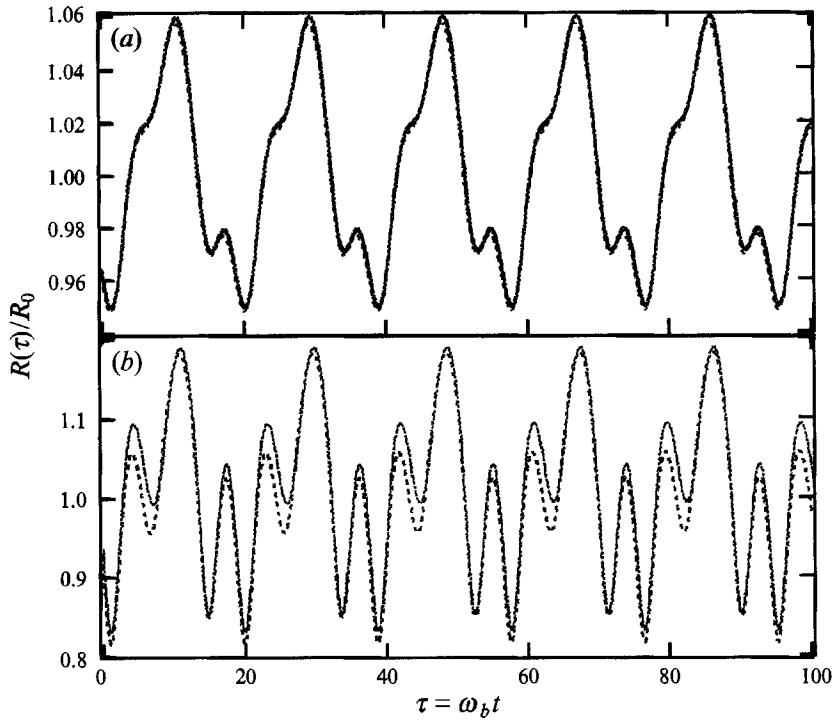


FIGURE 1. Radius, $R(\tau)/R_0$, is plotted against the non-dimensional time, $\tau = \omega_b t$, for a single bubble for (a) $P_n/\omega_b^2 R_0^2 = 0.04$ and (b) 0.08. $\omega_b/\omega_f = 3.0$, and $\nu/\omega_b R_0^2$ and $S/\rho\omega_b^2 R_0^3$ are for the water tunnel conditions. —, The numerical solution; ----, the approximate analytical solution.

For illustrative purposes, we select the values of the parameters $\nu/\omega_b R_0^2$ and $S/\rho\omega_b^2 R_0^3$ for the water tunnel conditions listed in the table 1. We chose to consider a single bubble subjected to an oscillating pressure at infinity containing a single frequency, ω_f , such that $\omega_b/\omega_f = 3.0$ for several values of $P_n/\omega_b^2 R_0^2$. Results obtained from (6) are compared to a numerical integration of the Rayleigh–Plesset equation (which uses a fourth-order Runge–Kutta scheme) in figure 1 for $P_n/\omega_b^2 R_0^2 = 0.04$ and 0.08. It can be seen that the present approximate analysis works very well for the smaller amplitude and begins to show some discrepancies at larger amplitude.

It was previously noted that (6) has a non-zero solution only at the harmonics of the excitation frequency. However, at present it is impossible to prove the uniqueness of the solution for nonlinear equations such as (6). The agreement demonstrated in figure 1 adds some confidence that the present solutions are unique.

A comparison of the spectra of $[1 - R(t)/R_0]$ is made in figure 2 for the case in which the $P_n/\omega_b^2 R_0^2$ and ω_b/ω_f values are 0.08 and 6 respectively. It can be seen that the present approximate solution agrees well with the numerical integration for frequencies at which the magnitude is significant. This indicates that most important features of the oscillation at weakly nonlinear conditions are incorporated in our approximate solution. Note that the radius oscillations occur at harmonics of the frequency of the pressure oscillation, ω_f . The excitation frequency, ω_f , is varied from $\omega_b/100$ to $2\omega_b$ for the purpose of calculating the frequency response of the bubble. Figure 3 shows the frequency response of a single bubble subjected to a pressure oscillation with a $P_n/\omega_b^2 R_0^2$ value of 0.02. The lines labelled [1] are the magnitudes of the response at the fundamental excitation frequency ω_f so that, in this case, the abscissa represents ω_f/ω_b .

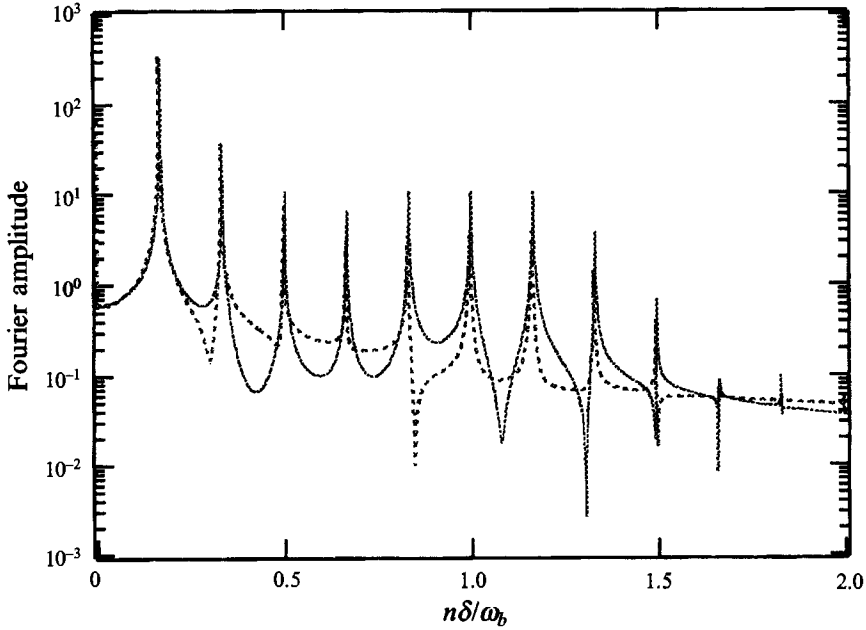


FIGURE 2. Comparison of the spectra of $[1 - R(\tau)/R_0]$ obtained for a single bubble from numerical integration of the Rayleigh-Plesset equation (—) and the present approximate (---) analysis. $P_n/\omega_b^2 R_0^2 = 0.08$, $\omega_b/\omega_f = 6.0$, and $\nu/\omega_b R_0^2$ and $S/\rho\omega_b^2 R_0^2$ are for the water tunnel conditions.

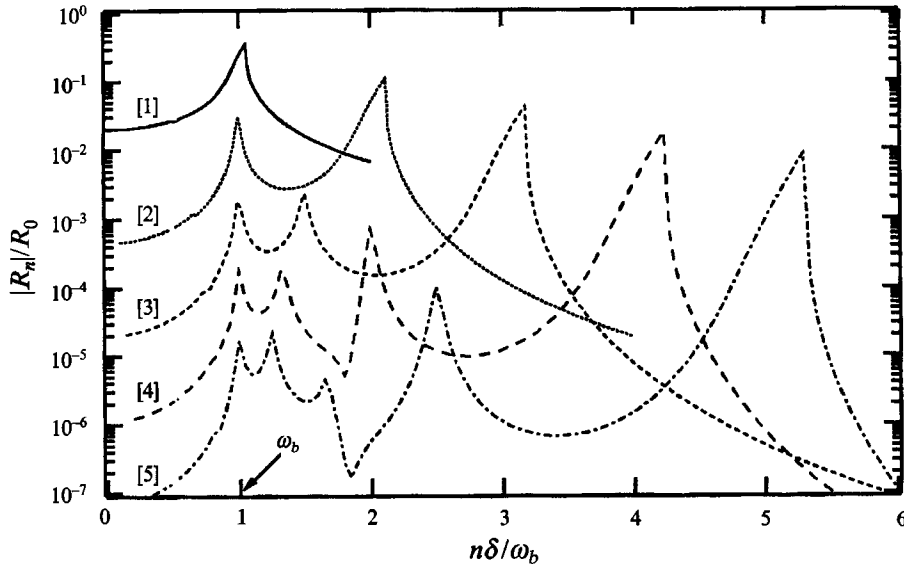


FIGURE 3. The frequency response of a single bubble: $|R_n|/R_0$ is plotted against the frequency ratio, $n\delta/\omega_b$, for the first five harmonics. $P_n/\omega_b^2 R_0^2 = 0.02$, and $\nu/\omega_b R_0^2$ and $S/\rho\omega_b^2 R_0^2$ are for the water tunnel conditions. The numbers in square brackets denote the order of the harmonic, and ω_b the bubble natural frequency.

The lines labelled [2] represent the magnitudes of the response at twice the excitation frequency and in this case the abscissa represents $2\omega_f/\omega_b$. A line labelled [m] represents the magnitude of the response at m times the excitation frequency and in this case the abscissa represents the frequency, $m\omega_f/\omega_b$. Thus, all the harmonics are plotted against

the actual reduced frequency, ω/ω_b , at which they occur. In viewing these results it should be recognized that those harmonics with magnitudes below a certain level are of dubious significance since higher-order nonlinearities could markedly alter those results. It can be seen that ω_b is the dominant frequency in the radius oscillation as would be expected from the linear analysis.

Eller & Flynn (1969) observed that for pressure oscillations with amplitude larger than a threshold value, the bubble radius oscillation will contain a subharmonic of order one-half. This can also be seen in Lauterborn's (1976) numerical calculation of the frequency response of a single bubble and in the third-order perturbation solution of Prosperetti (1974, 1975). The present solution does not give rise to subharmonics in the domain of its validity, i.e. $|R_n/R_0| \ll 1$. However, subharmonics are generated at stronger nonlinearities than considered in this paper and are considered as an indicator of the onset of vaporous cavitation (Vaughn 1968). Thus, the absence of subharmonics from our approximate solution does not invalidate our analysis when applied to weakly nonlinear oscillation of gaseous bubbles.

More accurate nonlinear solutions than the one described above (for example Prosperetti 1974, 1975) exist and have been reported in the literature. The value of present solution lies in its simplicity and the feasibility of incorporating it in an analysis of the collective response of a cloud of bubbles.

4. A bubble layer of finite thickness

The specific problem addressed in this paper is shown schematically in figure 4. Liquid containing bubbles is bounded by a flat wall which oscillates in a direction normal to itself at a frequency, ω_f . The resulting flow is assumed to be a function of x and t alone. A number of simplifying assumptions are used in order to obtain a soluble set of equations. The volume of liquid involved in condensation and evaporation during bubble oscillation has been ignored; this is reasonable in view of the large difference in the densities of the liquid and the vapour phases. The liquid has been assumed to be incompressible and the relative motion between the phases has been ignored. Both were found by d'Agostino & Brennen (1988) to have very little effect on important features such as the natural frequencies of the flow. The most important contribution of these effects is the damping that they cause at the resonant frequencies. This can be incorporated in the present solution by taking an appropriate value of the effective viscosity in place of the liquid viscosity used in the Rayleigh–Plesset equation.

The breakup and coalescence of bubbles are assumed not to occur for flows under weakly nonlinear excitation. Since relative motion has been neglected, the number of bubbles per unit liquid volume, η' , will remain constant under these assumptions; η' is also assumed to be piecewise uniform in the cases considered. Under these simplifying assumptions, the continuity and the momentum equations can be written in the form

$$\frac{\partial u}{\partial x} = \frac{\eta'}{(1 + \eta'\tau)} \frac{D\tau}{Dt}, \quad (11)$$

$$\rho \frac{Du}{Dt} = -(1 + \eta'\tau) \frac{\partial p}{\partial x}. \quad (12)$$

The equations (11) and (12) along with the Rayleigh–Plesset equation (3) relate the bubble size, the pressure in the flow and the flow velocity. Our analysis is used to obtain

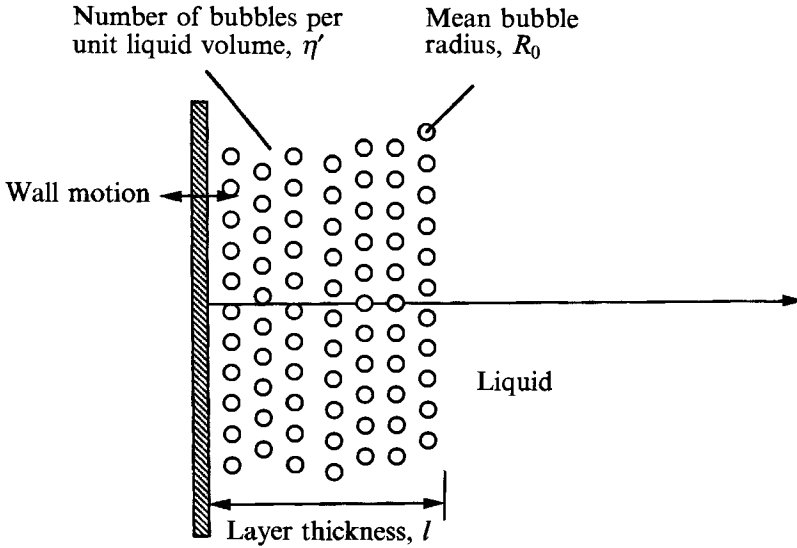


FIGURE 4. Schematic of the oscillating wall problem.

a single equation governing pressure oscillations in the layer. The solution to the problem represented by (11), (12) and (3) is obtained in Lagrangian coordinates, X and T , for which the above equations become

$$(1 + \eta'\tau) \frac{\partial u}{\partial X} = \eta' \frac{\partial \tau}{\partial T} \frac{\partial x}{\partial X} \tag{13}$$

and

$$\frac{\partial u}{\partial T} \frac{\partial x}{\partial X} = -(1 + \eta'\tau) \frac{1}{\rho} \frac{\partial p}{\partial X}. \tag{14}$$

The Lagrangian coordinates simplify the handling of convective nonlinearity. The velocity u can be written as

$$u = \partial x / \partial T. \tag{15}$$

Consistent with the structure of the solution sought, the relationship between the Lagrangian and the Eulerian coordinates, X and x , is written in the form

$$x = X + \sum_{n=1}^N \text{Re}(X_n(X) e^{in\delta T}), \tag{16}$$

and the bubble volume, τ , and pressure, P , are expressed by the expansions

$$\tau = \tau_0 + \sum_{n=1}^N \text{Re}(\tau_n(X) e^{in\delta T}) \tag{17}$$

and

$$\frac{P}{\rho} = P_0 + \sum_{n=1}^N \text{Re}(P_n(X) e^{in\delta T}). \tag{18}$$

The expansions (16), (17), (18) and (15) are substituted into (13) and coefficients of $e^{in\delta T}$ equated and some more simplifications are carried out to obtain

$$\frac{dX_n}{dX} = \alpha_0 \frac{\tau_n}{\tau_0} + \alpha_0^2 \sum_{j=1}^{n-1} \frac{(2j-n) \tau_j \tau_{n-j}}{2n \tau_0 \tau_0} + O(\alpha_0^3) \tag{19}$$

and
$$\frac{dP_n}{dX} = (1 - \alpha_0) n^2 \delta^2 X_n + O(\alpha_0^3). \tag{20}$$

The simple algebraic relation between the bubble radius, R , and the bubble volume, τ , namely $\tau = \frac{4}{3}\pi R^3$ leads to

$$\frac{\tau_n}{\tau_0} = 3 \frac{R_n}{R} + \frac{3}{2} \sum_{j=1}^{n-1} \frac{R_j}{R_0} \frac{R_{n-j}}{R_0} + 3 \sum_{j=1}^{N-n} \frac{\bar{R}_j}{R_0} \frac{R_{n+j}}{R_0}. \tag{21}$$

At this point we recall the approximate solution of the Rayleigh–Plesset equation given by (6) which may be written as

$$\frac{P_n}{\omega_b^2 R_0^2} = \Lambda(n) \frac{R_n}{R_0} + f_{n1}(X), \tag{22}$$

where
$$f_{n1}(X) = \sum_{j=1}^{n-1} \beta_1(n, j) \frac{R_j}{R_0} \frac{R_{n-j}}{R_0} + \sum_{j=1}^{N-n} \beta_2(n, j) \frac{\bar{R}_j}{R_0} \frac{R_{n+j}}{R_0}, \tag{23}$$

and $\beta_1(n, j)$ and $\beta_2(n, j)$ are given by (9) and (10). Using (19), (20), (21) and (22), the following equation governing the pressure oscillation in the bubble layer can be obtained

$$\begin{aligned} \frac{d^2(P_n/\omega_b^2 R_0^2)}{d(X/R_0)^2} &= \lambda_n^2 \frac{P_n}{\omega_b^2 R_0^2} \\ &+ \sum_{j=1}^{n-1} \frac{\lambda_n^2 \Lambda(n)}{\Lambda(j) \Lambda(n-j)} \left[\frac{1}{2} + 3\alpha_0 \frac{(2j-n)}{2n} - \frac{\beta_1(n, j)}{\Lambda(n)} \right] \frac{P_j}{\omega_b^2 R_0^2} \frac{P_{n-j}}{\omega_b^2 R_0^2} \\ &+ \sum_{j=1}^{N-n} \frac{\lambda_n^2 \Lambda(n)}{\Lambda(j) \Lambda(n+j)} \left[1 - \frac{\beta_2(n, j)}{\Lambda(n)} \right] \frac{\bar{P}_j}{\omega_b^2 R_0^2} \frac{P_{n+j}}{\omega_b^2 R_0^2}, \end{aligned} \tag{24}$$

where the parameter λ_n is given by

$$\lambda_n^2 = 3\alpha_0(1 - \alpha_0) \frac{(n\delta/\omega_b)^2}{\Lambda(n)}. \tag{25}$$

The solution of (24) (accurate up to second order) for a bubble layer of thickness l is as follows:

$$\begin{aligned} \frac{P_n}{\omega_b^2 R_0^2} &= \Lambda(n) [a_n \exp\{-\lambda_n X/R_0\} + b_n \exp\{\lambda_n(X-l)/R_0\}] \\ &+ \sum_{j=1}^{n-1} [\zeta_1(n, j) a_j a_{n-j} \exp\{-(\lambda_j + \lambda_{n-j}) X/R_0\} + \zeta_2(n, j) a_j b_{n-j} \exp\{-\lambda_j X/R_0 \\ &+ \lambda_{n-j}(X-l)/R_0\} + \zeta_2(n, j) b_j a_{n-j} \exp\{\lambda_j(X-l)/R_0 - \lambda_{n-j} X/R_0\} \\ &+ \zeta_1(n, j) b_j b_{n-j} \exp\{(\lambda_j + \lambda_{n-j})(X-l)/R_0\}] \\ &+ \sum_{j=1}^{N-n} [\zeta_3(n, j) \bar{a}_j a_{n+j} \exp\{-(\bar{\lambda}_j + \lambda_{n+j}) X/R_0\} \\ &+ \zeta_4(n, j) \bar{a}_j b_{n+j} \exp\{-\bar{\lambda}_j X/R_0 + \lambda_{n+j}(X-l)/R_0\} \\ &+ \zeta_4(n, j) \bar{b}_j a_{n+j} \exp\{\bar{\lambda}_j(X-l)/R_0 - \lambda_{n+j} X/R_0\} \\ &+ \zeta_3(n, j) \bar{b}_j b_{n+j} \exp\{(\bar{\lambda}_j + \lambda_{n+j})(X-l)/R_0\}], \end{aligned} \tag{26}$$

where

$$\zeta_1(n, j) = \frac{\lambda_n^2 \Theta(n, j)}{(\lambda_j + \lambda_{n-j})^2 - \lambda_n^2}, \tag{27}$$

$$\zeta_2(n, j) = \frac{\lambda_n^2 \Theta(n, j)}{(\lambda_j - \lambda_{n-j})^2 - \lambda_n^2}, \tag{28}$$

$$\zeta_3(n, j) = \frac{\lambda_n^2 \Gamma(n, j)}{(\bar{\lambda}_j + \lambda_{n+j})^2 - \lambda_n^2}, \tag{29}$$

$$\zeta_4(n, j) = \frac{\lambda_n^2 \Gamma(n, j)}{(\bar{\lambda}_j - \lambda_{n+j})^2 - \lambda_n^2}, \tag{30}$$

$$\Theta(n, j) = A(n) \left(\frac{1}{2} + 3\alpha_0 \frac{2j-n}{2n} \right) - \beta_1(n, j), \tag{31}$$

$$\Gamma(n, j) = A(n) - \beta_2(n, j), \tag{32}$$

and further details are included in Kumar (1991). In the linear approximation, the radius response may be written as

$$[R_n/R_0]_{\text{linear}} = a_n \exp\{-\lambda_n X/R_0\} + b_n \exp\{\lambda_n(X-l)/R_0\} \tag{33}$$

and we can proceed to evaluate $f_{n1}(X)$ from (23) by noting that it is consistent with the level of approximation to use (33) in the quadratic terms. Then the amplitude of radius oscillation, R_n/R_0 , (accurate up to second order) can be written as

$$\frac{R_n}{R_0} = \frac{P_n}{A(n) \omega_0^2 R_0^2} \frac{f_{n1}(X)}{A(n)}. \tag{34}$$

The solution (26) contains unknowns a_n and b_n which must be solved from the boundary conditions. The boundary conditions to be applied are (i) the given wall oscillation amplitude at $x = 0$ and (ii) the motion of the fluid at the edge of the layer is zero. Since the incompressible liquid outside the layer is infinite in extent, it must always be at rest at the lengthscales required for continuum modelling. The boundary conditions are applied to the following equation obtained from using (26) in (20):

$$\begin{aligned} \frac{\lambda_n X_n}{3\alpha_0 R_0} = & -a_n \exp\{-\lambda_n X/R_0\} + b_n \exp\{\lambda_n X/R_0\} \\ & + \sum_{j=1}^{n-1} [-\kappa_1(n, j) a_j a_{n-j} \exp\{-(\lambda_j + \lambda_{n-j}) X/R_0\} \\ & - \kappa_2(n, j) a_j b_{n-j} \exp\{-\lambda_j X/R_0 + \lambda_{n-j}(X-l)/R_0\} \\ & + \kappa_2(n, j) b_j a_{n-j} \exp\{\lambda_j(X-l)/R_0 - \lambda_{n-j} X/R_0\} \\ & + \kappa_1(n, j) b_j b_{n-j} \exp\{(\lambda_j + \lambda_{n-j})(X-l)/R_0\}] \\ & + \sum_{j=1}^{N-n} [-\kappa_3(n, j) \bar{a}_j a_{n+j} \exp\{-(\bar{\lambda}_j + \lambda_{n+j}) X/R_0\} \\ & - \kappa_4(n, j) \bar{a}_j b_{n+j} \exp\{-\bar{\lambda}_j X/R_0 + \lambda_{n+j}(X-l)/R_0\} \\ & + \kappa_4(n, j) \bar{b}_j a_{n+j} \exp\{\bar{\lambda}_j(X-l)/R_0 - \lambda_{n+j} X/R_0\} \\ & + \kappa_3(n, j) \bar{b}_j b_{n+j} \exp\{(\bar{\lambda}_j + \lambda_{n+j})(X-l)/R_0\}], \tag{35} \end{aligned}$$

where

$$\kappa_1 = \frac{\lambda_n(\lambda_j + \lambda_{n-j})\Theta(n, j)}{A(n)((\lambda_j + \lambda_{n-j})^2 - \lambda_n^2)}, \quad (36)$$

$$\kappa_2 = \frac{\lambda_n(\lambda_j - \lambda_{n-j})\Theta(n, j)}{A(n)((\lambda_j - \lambda_{n-j})^2 - \lambda_n^2)}, \quad (37)$$

$$\kappa_3 = \frac{\lambda_n(\bar{\lambda}_j + \lambda_{n+j})\Gamma(n, j)}{A(n)((\bar{\lambda}_j + \lambda_{n+j})^2 - \lambda_n^2)}, \quad (38)$$

$$\kappa_4 = \frac{\lambda_n(\bar{\lambda}_j - \lambda_{n+j})\Gamma(n, j)}{A(n)((\bar{\lambda}_j - \lambda_{n+j})^2 - \lambda_n^2)}. \quad (39)$$

The constants ζ_1 – ζ_4 and κ_1 – κ_4 can be evaluated using their definitions and given fluid and bubble properties. Thus applying the boundary conditions, a set of nonlinear algebraic equations is obtained for a_n and b_n . These are solved using a Newton–Raphson scheme. Since (35) is similar to (6), it can be seen that the solution is independent of the way in which the frequency domain is discretized. Having calculated a_n and b_n , $P_n/\omega_b^2 R_0^2$ can be calculated using (26) and R_n/R_0 obtained using (34) while using (33) and (23) to evaluate $f_{n1}(X)$. Also, both $P_n/\omega_b^2 R_0^2$ and R_n/R_0 appear only at the harmonics of the frequency of wall oscillation, ω_f . Thus the software may be written so as to evaluate only the non-zero response amplitudes, at the harmonics of excitation frequency. Calculation of up to 20 harmonics was found to be sufficient, harmonics of higher order being negligible. The frequency response of the bubbly layer was calculated by varying the wall oscillation frequency from $\omega_b/100$ to $2\omega_b$ and the resulting amplitudes of $P_n/\omega_b^2 R_0^2$ and R_n/R_0 are plotted as functions of the reduced frequency, $n\delta/\omega$ in similar manner to that in figure 3. Calculation is carried out for two sets of values listed in table 1. A convenient reference case consists of water tunnel conditions plus a void fraction, α_0 of 0.02 and wall oscillation amplitude $(X_n)/R_0$ of 0.02. The ocean conditions are used to examine the effect of varying the viscous and surface tension parameters.

It is known that presence of a lengthscale such as a finite thickness of the bubble layer results in characteristic natural frequencies of the bubble cloud (d’Agostino & Brennen 1988; Omta 1987). It has also been shown that the lowest characteristic natural frequency of the cloud, ω_1 dominates the frequency response (d’Agostino & Brennen 1988). Here, we shall explore the influence of weak nonlinear effects on these phenomena.

It can be easily verified that the natural frequencies of such a bubble layer are given in the absence of damping by

$$\frac{\omega_n}{\omega_b} = \left[1 + \frac{3\alpha_0(1-\alpha_0)}{n^2\pi^2} \left(\frac{l}{R_0} \right)^2 \right]^{-\frac{1}{2}}; \quad n = 1, 2, \dots \quad (40)$$

With damping, the natural frequencies of the cloud differ from the above values by only a small amount. A typical frequency response of a bubble cloud of finite thickness is shown in figure 5 where the water tunnel conditions (table 1) have been used. The amplitudes of harmonics above the first and the second have been omitted since they are negligible. The first harmonic is similar to that predicted by the linear solution. For both the pressure and the radius response, significant amplitudes of oscillation can be observed at the characteristic natural frequencies of the cloud with the response at the lowest cloud natural frequency being dominant. Note that the response at the characteristic natural frequencies close to ω_b is overwhelmed by the response

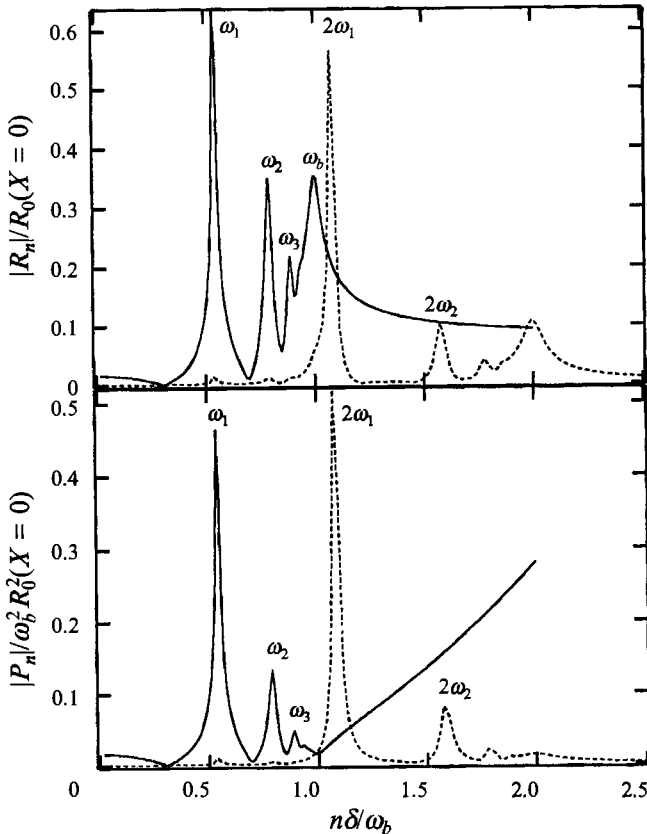


FIGURE 5. The frequency response of a bubble layer of finite thickness: $|R_n|/R_0(X=0)$ and $|P_n|/\omega_b^2 R_0^2(X=0)$ are plotted against the frequency ratio, $n\delta/\omega_b$, for first two harmonics (—, fundamental; ---, second). $X_n(0)/R_0 = 0.02$, $\alpha_0 = 0.02$, $l/R_0 = 20$, and $\nu/\omega_b R_0^2$ and $S/\rho\omega_b^2 R_0^3$ are for the water tunnel conditions.

modification due to the proximity of ω_b , making it impossible to distinguish the peaks at characteristic natural frequencies close to ω_b . Furthermore, the response at the second harmonic of the lowest characteristic natural frequency (at $2\omega_1$) is greater than the response of the fundamental at other natural frequencies ($\omega_2, \omega_3, \dots$) of the bubble cloud. The most significant frequency is the lowest natural frequency of the cloud and even weak nonlinear effects cause the harmonics of this frequency to dominate the other natural cloud frequencies. Since, the second harmonic response at $2\omega_1$ is not highly damped, there remain some important high frequencies such as $2\omega_1$ in the response and all high-frequency response cannot be ruled out. This is, perhaps, the most important nonlinear phenomenon to add to the conclusions of the linearized analysis of d'Agostino & Brennen (1988). Also, the pressure increases with excitation frequency for excitation frequencies larger than ω_b . This indicates that the oscillations are too fast to follow for the bubbles, which do not respond as quickly due to their virtual mass, and the whole bubble layer moves as a homogeneous medium in response to the oscillating wall.

Following d'Agostino & Brennen (1988), we can consider the solution to be divided into three different regimes, namely: *sub-resonant* ($0 < \omega_f < \omega_1$), *trans-resonant* ($\omega_1 < \omega_f < \omega_b$) and *super-resonant* ($\omega_f > \omega_b$). The first harmonic of the radius oscillation

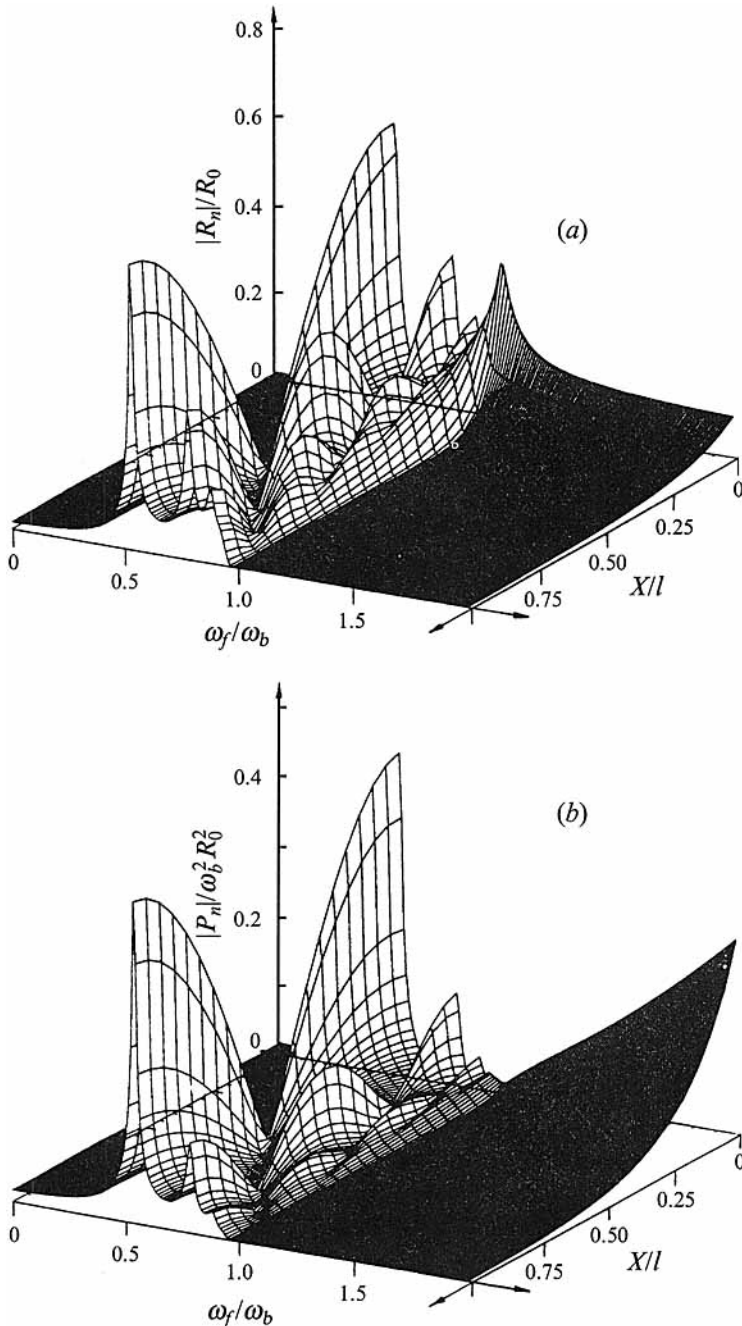


FIGURE 6. The frequency response of a bubble layer of finite thickness: (a) $|R_n|/R_0$ and (b) $|P_n|/\omega_b^2 R_0^2$ for the fundamental harmonic are plotted against the frequency ratio, ω_f/ω_b , and the distance from the oscillating wall, X/l , for the first harmonic. $X_n(0)/R_0 = 0.02$, $\alpha_0 = 0.02$, $l/R_0 = 20$, and $\nu/\omega_b R_0^2$ and $S/\rho\omega_b^2 R_0^3$ are for the water tunnel conditions.

and the pressure oscillation are shown as surface plots in figure 6 as functions of the frequency ratio, ω_f/ω_b and distance from the wall, X/l so that we may illustrate the frequency response of the cloud away from the oscillating wall. In the cases of the sub-resonant and trans-resonant excitation, the amplitudes of oscillation form standing

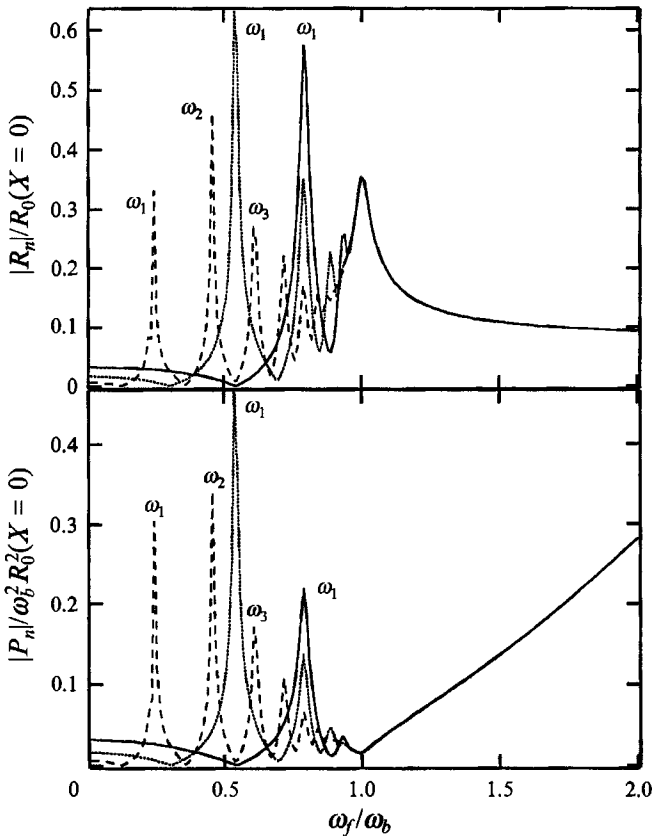


FIGURE 7. The effect of a change in the thickness of the bubble layer, l/R_0 , on the fundamental harmonic: $|R_n|/R_0(X=0)$ and $|P_n|/\omega_b^2 R_0^2(X=0)$ for the fundamental harmonic are plotted against the frequency ratio, ω_f/ω_b . $X_n(0)/R_0 = 0.02$, $\alpha_0 = 0.02$, and $\nu/\omega_b R_0^2$ and $S/\rho\omega_b^2 R_0^3$ are for the water tunnel conditions. —, $l/R_0 = 10$; \cdots , 20; ---, 50.

wave patterns and the amplitudes decay slowly with distance from the wall. In the case of super-resonant excitation, the response is seen to rapidly decay with distance from the wall.

Comparing the rapid decay of the response away from the centre of the spherical cloud (d'Agostino & Brennen 1988) with the present solution for sub-resonant and trans-resonant excitation, it appears that the strong decay at a distance from the cloud centre in the case of a spherical cloud is caused by attenuation due to spherical divergence. In other words, the response at the centre of the spherical cloud is much stronger than the response at the boundary of the cloud due to focusing of the spherically symmetric disturbance. Thus, for sub-resonant and trans-resonant excitations the magnitude of the response is determined by the geometry of the bubble cloud and the excitation. The bubbles have ample time to react to the excitation and the bubble dynamics significantly influence the response throughout the layer. In the case of the super-resonant excitation the response is seen to decay rapidly with the distance from the oscillating wall in the same way as it decayed rapidly with the distance from the boundary of a spherical cloud (d'Agostino & Brennen 1988). Thus, in the case of super-resonant excitation the response gets weaker with increasing distance from the source of excitation and the bubble dynamics do not play any significant role except in the dissipation of the input energy.

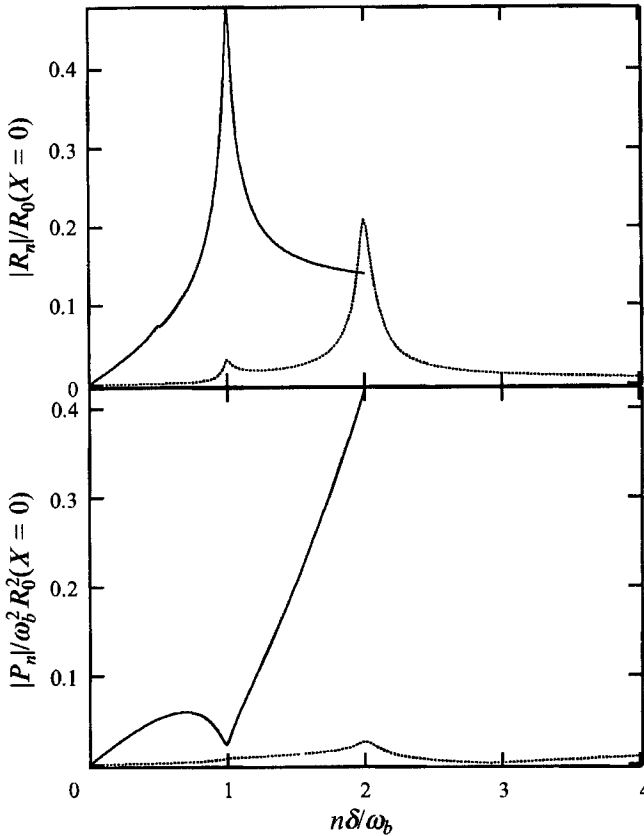


FIGURE 8. The frequency response of a semi-infinite layer: $|R_n|/R_0(X=0)$ and $|P_n|/\omega_b^2 R_0^2(X=0)$ for the first two harmonics are plotted against the frequency ratio, $n\delta/\omega_b$ (—, fundamental; ····, second harmonic). $X_n(0)/R_0 = 0.03$, $\alpha_0 = 0.02$, and $\nu/\omega_b R_0^2$ and $S/\rho\omega_b^2 R_0^3$ are for the water tunnel conditions.

The effect of variation in the thickness of the bubble layer, l/R_0 , for a given value of the void fraction will be examined next. Note that thickening the layer will increase the size of the frequency interval containing the natural frequencies of the layer, $[\omega_1, \dots, \omega_b]$, by lowering the lowest characteristic natural frequency, ω_1 . Figure 7 illustrates the changes in frequency response of the layer due to the increase in its thickness. It is clear that the change in the thickness of the layer does not influence the frequency response for super-resonant excitation and for excitation frequencies close to ω_b . The amplitude of oscillation is a maximum at the lowest cloud natural frequency, ω_1 , in cases for which ω_1 is greater than $0.5\omega_b$. However, the amplitude of oscillation at ω_2 is greater than at ω_1 in the case for which ω_1 is about $0.25\omega_b$. Thus, it appears that the amplitude of oscillation at a cloud natural frequency increases as that cloud natural frequency gets closer to about $0.5\omega_b$. The response at the second harmonic followed essentially the same pattern (Kumar 1991). When the cloud natural frequencies move to values much less than $0.5\omega_b$ with increase in the thickness of the layer, the amplitude of oscillation at these cloud natural frequencies decreases to the values given in the infinitely thick layer solution (figure 8). It can be noted from figure 8 that the pressure oscillation second harmonic at $2\omega_b$ is almost the same as the fundamental harmonic at ω_b for the semi-infinite layer of identical bubbles.

Turning to the effect of the void fraction, figure 9 presents results for several values

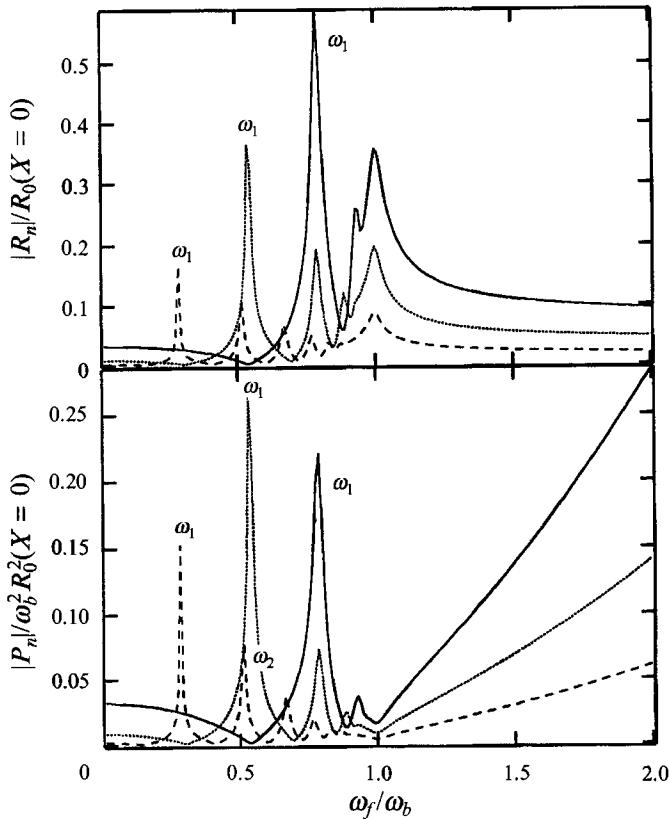


FIGURE 9. The effect of change in the void fraction, α_0 , on the fundamental harmonic: $|R_n|/R_0(X=0)$ and $|P_n|/\omega_b^2 R_0^2(X=0)$ for the fundamental harmonic are plotted against the frequency ratio, ω_f/ω_b . $X_n(0)/R_0 = 0.02$, $\alpha_0 = 0.02$ and $l/R_0 = 20$. $\nu/\omega_b R_0^2$ and $S/\rho\omega_b^2 R_0^2$ are for the water tunnel conditions. —, $\alpha_0 = 0.005$; \cdots , 0.020 ; ---, 0.100 .

of α_0 . An increase in void fraction reduces the characteristic natural frequencies, as is clear from (40). Note that the amplitude of oscillation is reduced by an increase in the void fraction for excitation frequencies close to and greater than ω_b . Two other features of figure 9 are noteworthy. First, the amplitude of pressure oscillation at ω_1 is larger for the void fraction of 0.020 than for the void fraction of 0.005. A possible reason for this is the proximity of ω_1 to $0.5\omega_b$ for the void fraction of 0.020. Second, the amplitude of pressure oscillation at ω_1 is larger than that at ω_2 for the void fraction of 0.1 whereas the response at ω_2 is greater than the response at ω_1 for $\alpha_0 = 0.02$ and $l/R_0 = 50$ (seen earlier in figure 7). Thus, it appears that both the proximity of the cloud natural frequencies to $0.5\omega_b$ and the void fraction influence the relative amplitudes of oscillation at ω_1 and ω_2 .

The effect of changing the viscous and surface tension parameters is illustrated in figure 10 for the fundamental harmonic. This contains a comparison between the frequency response for the ocean conditions and the response for the water tunnel conditions noted earlier. Larger viscous and surface tension parameters (at water tunnel conditions) tend to inhibit bubble oscillations and so the response curves for ocean conditions exhibit sharper peaks and troughs.

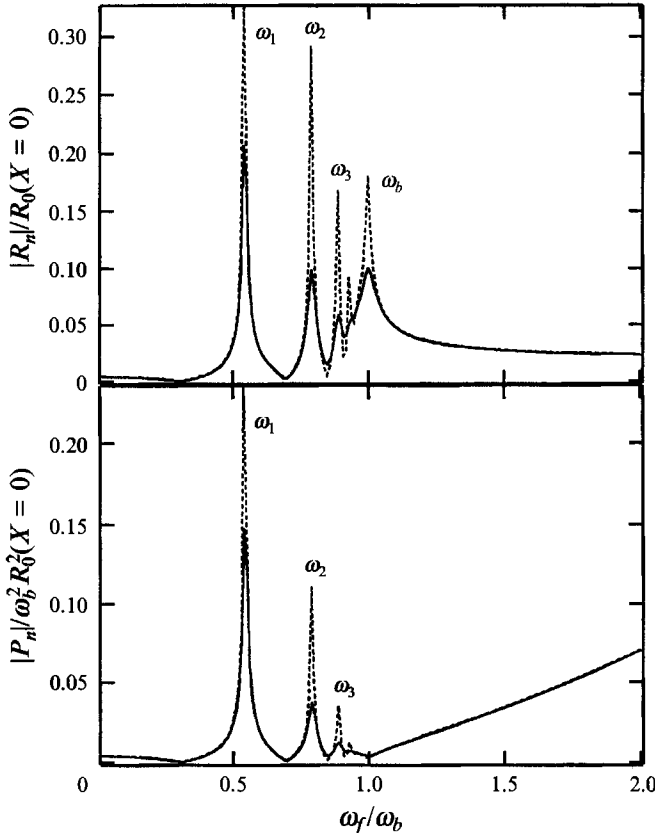


FIGURE 10. The effect of a change in the ambient conditions ($\nu/\omega_b R_0^2$ and $S/\rho\omega_b^2 R_0^3$) on the fundamental harmonic: $|R_n|/R_0(X=0)$ and $|P_n|/\omega_b^2 R_0^2(X=0)$ for the fundamental harmonic are plotted against the frequency ratio, ω_f/ω_b . $X_n(0)/R_0 = 0.005$, $\alpha_0 = 0.02$, $l/R_0 = 20$, and $\nu/\omega_b R_0^2$ and $S/\rho\omega_b^2 R_0^3$ are for the water tunnel (—) and the ocean (----) conditions.

5. A semi-infinite layer with bubble size distribution

Most of the research efforts in modelling bubbly mixtures so far have assumed bubbly mixtures of identical bubbles. In most practical circumstances, uniformly sized bubbles are very difficult if not impossible to achieve. Moreover, cavitation nuclei in water have a distribution of bubble sizes ranging over several orders of magnitude (Gates & Acosta 1978).

In this section, we present a weakly nonlinear model of flows of such bubbly mixtures. Since the flow now has a number of length and time scales in terms of the bubble radii and their natural periods, we can expect different mechanisms causing interactions between the different timescales. We shall find a new mechanism for frequency dispersion called *harmonic cascading*.

In this solution we assume that the bubble number density distribution, $\eta(R_0)$, is known and that it is piecewise uniform. A continuum of bubble radii is assumed. Then, the number of bubbles per unit liquid volume with equilibrium size between R_0 and $R_0 + dR_0$ is $\eta(R_0)dR_0$. The volume of bubbles per unit liquid volume is

$$\frac{\alpha}{1-\alpha} = \int_{R_m}^{R_M} \eta(R_0) \tau dR_0, \tag{41}$$

where the volume of the bubble, τ , is given by (17) and R_m and R_M are minimum and

maximum equilibrium bubble radii present in the layer. Thus, the number of bubbles per unit total volume with equilibrium radius between R_0 and $R_0 + dR_0$, can be written as

$$\eta^*(R_0) dR_0 = \eta(R_0) (1 - \alpha) dR_0 = \frac{\eta(R_0) dR_0}{1 + \int_{R_m}^{R_M} \eta(R_0) \tau dR_0}. \tag{42}$$

Substituting the expansion (17) into (41) we obtain

$$\int_{R_m}^{R_M} \eta(R_0) \tau dR_0 = \frac{\alpha_0}{1 - \alpha_0} + \sum_{n=1}^N \text{Re}(A_n e^{in\delta T}), \tag{43}$$

where

$$A_n = \int_{R_m}^{R_M} \eta(R_0) \tau_n dR_0. \tag{44}$$

We use a dispersed-phase number continuity equation (DPNC) to ensure mass and number conservation. Assuming the liquid to be incompressible, it follows that if the bubbles are neither created nor destroyed then

$$\frac{D}{Dt} \int_{R_m}^{R_M} \eta^*(R_0) dR_0 + \frac{\partial u}{\partial x} \int_{R_m}^{R_M} \eta^*(R_0) dR_0 = 0. \tag{45}$$

Assuming that the number density per unit total volume is conserved, (45) reduces to

$$\frac{D\eta^*(R_0)}{Dt} + \eta^*(R_0) \frac{\partial u}{\partial x} = 0, \tag{46}$$

and the corresponding momentum equation is

$$\rho(1 - \alpha) \frac{Du}{Dt} = - \frac{\partial p}{\partial x}. \tag{47}$$

The solution to the problem represented by (3), (42), (46) and (47) was solved in Lagrangian coordinates, X and T , using a method parallel to that described in §4. The above equations ((46) and (47)) become

$$\frac{\partial \eta^*(R_0)}{\partial T} \frac{\partial x}{\partial X} + \eta^*(R_0) \frac{\partial u}{\partial X} = 0 \tag{48}$$

and

$$\rho \frac{\partial u}{\partial T} \frac{\partial x}{\partial X} = - \frac{1}{1 - \alpha} \frac{\partial P}{\partial X}. \tag{49}$$

Using (41)–(44) it can be seen that the simplified form of the DPNC equation (46) and the momentum equation (47) depend upon the integral measures of the bubble volume oscillations and bubble size distribution, A_n , and not on the bubble size distribution density $\eta(R_0)$. The approximate solution to the Rayleigh–Plesset equation (6) can be used to express the A_n as functions of the P_n . Thus we have three unknowns – pressure oscillation, flow velocity and the integral measure, A_n , to be solved from three equations. Following a methodology very similar to that in the §4, these three equations are used to obtain the following governing equation for the pressure oscillations in the layer (Kumar 1991):

$$\frac{d^2(P_n/\omega_r^2 l_r^2)}{d(X/l_r)^2} = \lambda_n^2 \frac{P_n}{\omega_r^2 l_r^2} + \sum_{j=1}^{n-1} \psi(n, j) \frac{P_j}{\omega_r^2 l_r^2} \frac{P_{n-j}}{\omega_r^2 l_r^2} + \sum_{j=1}^{N-n} \theta(n, j) \frac{\bar{P}_j}{\omega_r^2 l_r^2} \frac{P_{n+j}}{\omega_r^2 l_r^2}, \tag{50}$$

where
$$\lambda_n^2 = (1 - \alpha_0)^2 \left(\frac{n\delta}{\omega_r}\right)^2 \phi'(n), \tag{51}$$

$$\psi(n, j) = (1 - \alpha_0)^2 \left(\frac{n\delta}{\omega_r}\right)^2 \left[\psi'(n, j) + (1 - \alpha_0) \frac{2j - n}{2n} \phi'(j) \phi'(n - j) \right], \tag{52}$$

$$\theta(n, j) = (1 - \alpha_0)^2 \left(\frac{n\delta}{\omega_r}\right)^2 \theta'(n, j), \tag{53}$$

$$\phi'(n) = \int_{R_m}^{R_M} \frac{3\eta(R_0) \tau_0 \omega_r^2 l_r^2}{A(n) \omega_b^2 R_0^2} dR_0, \tag{54}$$

$$\psi'(n, j) = \int_{R_m}^{R_M} \frac{3\eta(R_0) \tau_0 \omega_r^4 l_r^4}{A(j) A(n - j) \omega_b^4 R_0^4} \left[\frac{1}{2} - \frac{\beta_1(n, j)}{A(n)} \right] dR_0, \tag{55}$$

$$\theta'(n, j) = \int_{R_m}^{R_M} \frac{3\eta(R_0) \tau_0 \omega_r^4 l_r^4}{A(j) A(n + j) \omega_b^4 R_0^4} \left[1 - \frac{\beta_2(n, j)}{A(n)} \right] dR_0. \tag{56}$$

Equation (50) has the following approximate solution (accurate to the second order and obtained in manner similar to the solution to (24) given by (26)):

$$\begin{aligned} \frac{P_n}{\omega_r^2 l_r^2} = & c_n e^{-\lambda_n X/l_r} + \sum_{j=1}^{n-1} \frac{\psi(n, j) c_j c_{n-j}}{(\lambda_j + \lambda_{n-j})^2 - \lambda_n^2} e^{-(\lambda_j + \lambda_{n-j}) X/l_r} \\ & + \sum_{j=1}^{N-n} \frac{\theta(n, j) \bar{c}_j c_{n+j}}{(\bar{\lambda}_j + \lambda_{n+j})^2 - \lambda_n^2} e^{-(\bar{\lambda}_j + \lambda_{n+j}) X/l_r}. \end{aligned} \tag{57}$$

Using the solution given by (57) and the momentum equation (Kumar 1991) the following relation for the conditions at the wall may be obtained:

$$\begin{aligned} -(1 - \alpha_0) \left(\frac{n\delta}{\omega_r}\right)^2 \frac{X_n(0)}{l_r} = & \lambda_n c_n + \sum_{j=1}^{n-1} \frac{(\lambda_j + \lambda_{n-j}) \psi(n, j) c_j c_{n-j}}{(\lambda_j + \lambda_{n-j})^2 - \lambda_n^2} \\ & + \sum_{j=1}^{N-n} \frac{(\bar{\lambda}_j + \lambda_{n+j}) \theta(n, j) \bar{c}_j c_{n+j}}{(\bar{\lambda}_j + \lambda_{n+j})^2 - \lambda_n^2}. \end{aligned} \tag{58}$$

In the case of identical bubbles, we have

$$\eta(R_0) = \eta' \delta(R_0 - R'_0), \tag{59}$$

where η' is the total number of bubbles per unit liquid volume and R'_0 is the radius of the bubbles. It can be seen that the above result reduces to that for identical bubbles.

For illustration we examine a bubble layer containing bubbles of radii between 10.0 and 100.0 μm under the water tunnel conditions. The largest natural frequency of the bubble and the largest bubble radius present in cloud are convenient choices for the reference frequency, ω_r and the reference lengthscale, l_r , respectively. In the sample calculations the coefficients, $\phi'(n)$, $\psi'(n, j)$ and $\theta'(n, j)$ were evaluated using (54), (55) and (56) respectively. The integrals were evaluated numerically using the trapezoidal rule and Richardson extrapolation was used to estimate the value of the integral for zero step size. The parameters A_n , $\beta_1(n, j)$ and $\beta_2(n, j)$ were calculated from (8), (9) and (10), and λ_n , $\psi(n, j)$ and $\theta(n, j)$ could then be calculated using (51)–(53). Equation (58) was then solved using a Newton–Raphson scheme to calculate the constants c_n for a given amplitude of wall oscillation, $X_n(0)/l_r$. Knowing c_n , the amplitude of pressure oscillation could be calculated from (57). Using this solution, the values of R_n/R_0 were

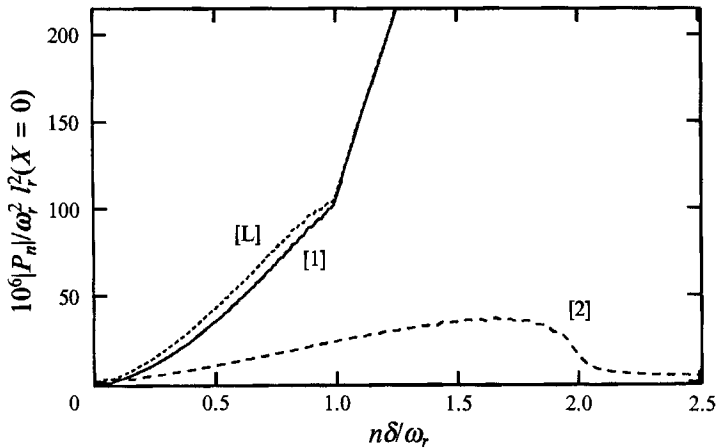


FIGURE 11. The frequency response of a bubbly layer with a given size distribution of bubbles: $|P_n|/\omega_r^2 l_r^2(X=0)$ is plotted against the frequency ratio, $n\delta/\omega_r$, for the first two harmonics ([1], [2]) and the linear solution ([L]) for $m=3$. $X_n(0)/l_r = 0.0002$, $\alpha_0 = 0.05$, and ambient conditions are for the water tunnel.

calculated for different values of R_0 using (34) and the amplitude of R_n/R_0 is checked to ensure that it is less than unity. Note that (58) is similar in structure to (6) and also its solution is non-zero only at harmonics of the excitation frequency. Once again calculations of up to 20 harmonics were found to be sufficient.

Numerical results were computed for a number of typical cases. For each case the results were obtained for the size distribution density parameter, $m=2, 3, 4$ (see (1)) and the value of N^* was adjusted to obtain the required value of the void fraction. It is important to note that a larger value of m implies increasing the number of small bubbles relative to the number of large bubbles. The results for six different cases were obtained in order to investigate the effect of changes in void fraction, ambient conditions and amplitude of wall oscillation.

A typical frequency response of the cloud is shown in figure 11 for the water tunnel conditions (table 1). This illustrates the features of the frequency response common to all cases. The amplitude of pressure oscillation for the fundamental and the second harmonic, which are marked [1] and [2] respectively, as well as the solution obtained from the linearized analysis, which is marked [L], are shown. Amplitudes of higher harmonics were found to be negligible. The frequency ratio is the ratio of the actual frequency at which the response occurs to the reference frequency, in the same way as figure 3 was constructed. It is seen that the amplitude of first harmonic of pressure oscillation increases with increasing excitation frequency. The reason for this is that there is a larger number of smaller bubbles, for which the natural frequency of the bubble is larger. Thus for larger frequency ratios (excitation frequencies) a larger number of bubbles are excited at their natural frequency thus leading to an increase in the amplitude of the pressure oscillation. The sub-resonant excitation of small bubbles and super-resonant excitation of large bubbles also contributes to an increase in the amplitude of pressure oscillation. A kink can be seen in the fundamental harmonic at an excitation frequency of ω_r (figure 11). This is because, for excitation frequencies larger than ω_r , the pressure oscillation is caused solely by the super-resonant excitation of bubbles in the layer.

Figure 12 presents the amplitude of pressure oscillation for the first and the second harmonic as a function of the frequency ratio, ω/ω_r and the distance from the wall,

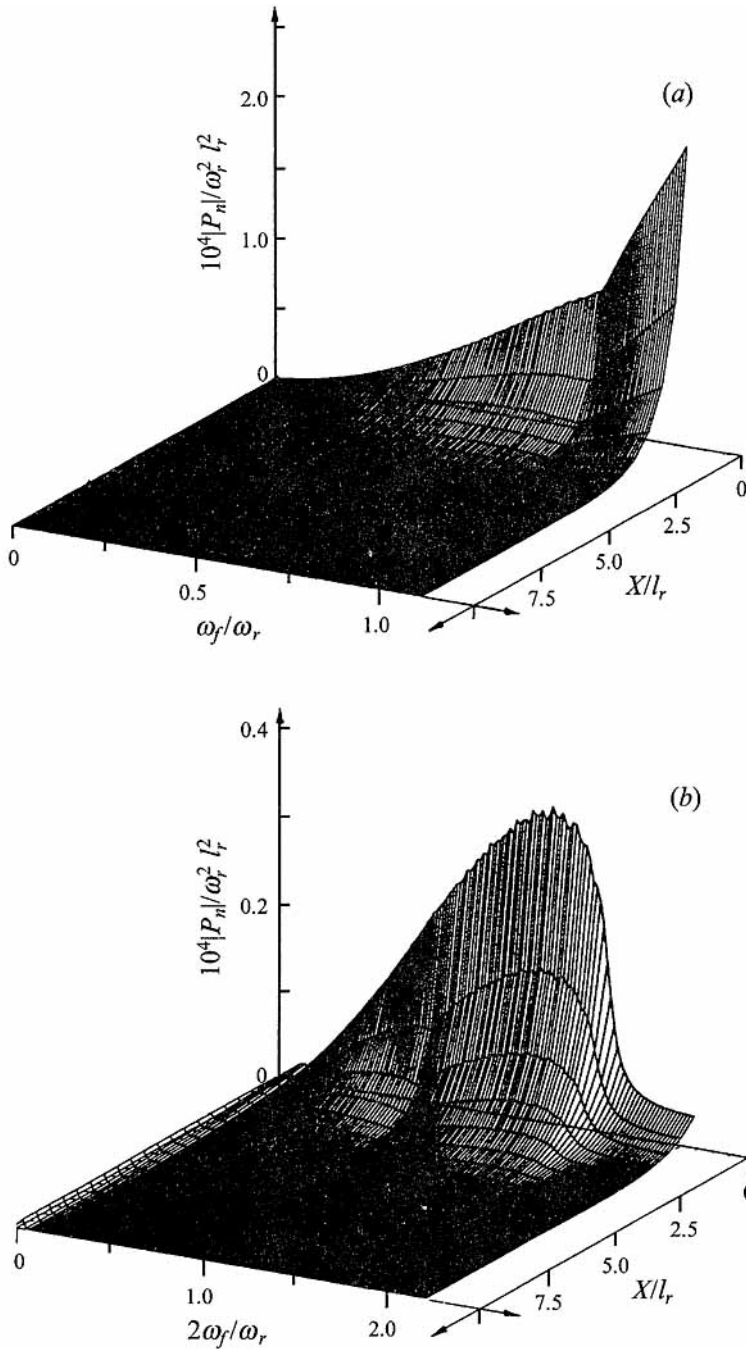


FIGURE 12. The frequency response of a bubbly layer with a given size distribution of bubbles: $|P_n|/\omega_r^2 l_r^2$ for the (a) first and (b) second harmonic is plotted against the distance from the wall, X/l_r , and frequency ratios (a) ω_f/ω_r and (b) $2\omega_f/\omega_r$, respectively. $X_n(0)/l_r = 0.0002$, $\alpha_0 = 0.05$, $m = 3$ and ambient conditions are for the water tunnel.

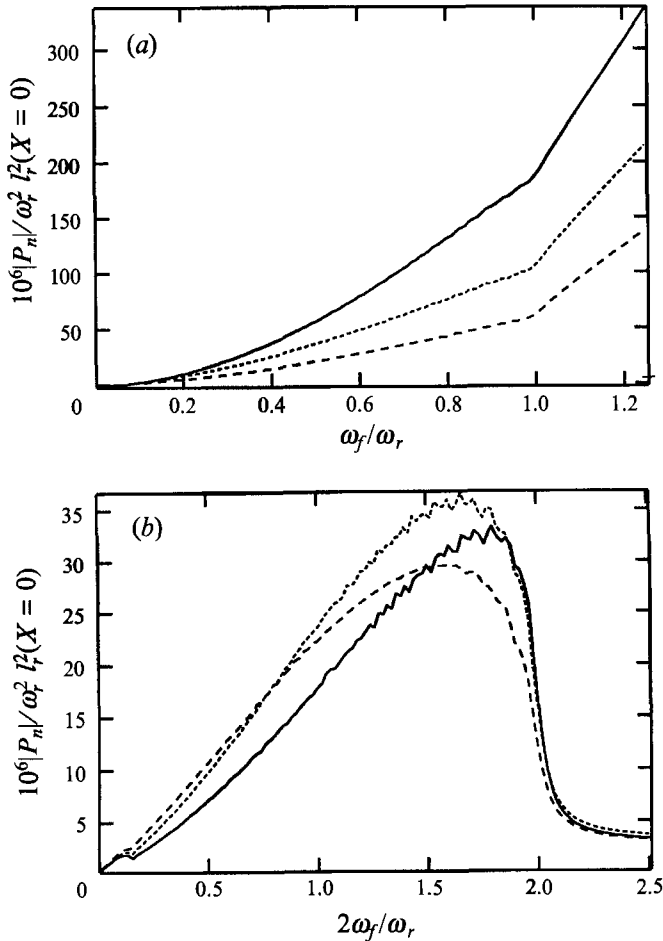


FIGURE 13. The effect of variation in the bubble size density distribution slope, m , on (a) the first and (b) the second harmonics: $|P_n|/\omega_f^2 l_r^2 (X=0)$ is plotted against frequency ratios (a) ω_f/ω_r and (b) $2\omega_f/\omega_r$, respectively. $X_n(0)/l_r = 0.0002$, $\alpha_0 = 0.05$ and ambient conditions are for the water tunnel. —, $m = 2$; \cdots , 3; ---, 4.

X/l_r . It is quite clear that the pressure oscillation decays rapidly away from the wall, decaying to very small values at a distance of $4l_r$ from the wall. The response was also seen to decay rapidly away from the wall for a semi-infinite layer of identical bubbles.

When the wall is oscillated at a frequency, ω_f , bubbles with their natural frequency equal to ω_f are excited with the largest amplitude. Because of the nonlinearity present in the system, the flow variables oscillate at the harmonics of the excitation frequency, ω_f . Thus, the pressure oscillation at $2\omega_f$ excites bubbles with the natural frequency equal to $2\omega_f$ and since, the number of bubbles with the natural frequency, $2\omega_f$, is larger than the number of bubbles with the natural frequency, ω_f , the response resulting from the bubbles with natural frequency $2\omega_f$ may be significant and may be larger for larger values of m . In other words, the excitation may cascade towards higher frequencies. This means that an excitation at small frequencies may elicit a strong response at high frequencies. We shall refer to this mechanism as *harmonic cascading*.

The ratio of the amplitude of the second harmonic to the amplitude of the first harmonic increases for larger values of the parameter m (figure 13). This could be expected from the above description of the mechanism of harmonic cascading. Note

that the linear solution is larger than the first harmonic (figure 11) and the difference between the linear solution and the first harmonic is also seen to be larger for larger values of m . For excitation frequencies larger than the reference frequency, ω_r , the amplitude of the second harmonic is very small and the difference between the linear and nonlinear solutions is also very small (figure 11). This could be anticipated since ω_r is the highest natural frequency present in the cloud and the effect of harmonic cascading is expected to decrease for wall oscillation frequencies larger than $0.5\omega_r$. For excitation frequencies up to $0.5\omega_r$, harmonic cascading remains an important effect with the amplitude of second harmonic becoming larger than the amplitude of first harmonic for $m = 4$. For excitation frequencies larger than $0.5\omega_r$, the increase is due to the collective response of the bubbles to the excitation. It also appears that an increase in the value of m reduces the amplitude of the first harmonic and affects the second harmonic only weakly (figure 13). For a given value of the void fraction, the number of bubbles is larger for larger values of m and the reduction in the amplitude of pressure oscillations may be caused by the increased damping in the system due to the larger number of bubbles. The weaker response for increased void fraction for a layer of identical bubbles may also be caused by an increase in the number of bubbles. Note that the amplitude of the second harmonic is not strongly affected by changes in the value of m .

The effect of changes in ambient conditions on the frequency response is not a strong one. However, it does appear that the ocean conditions do promote slightly stronger harmonic cascading. This may be explained as follows. The super-resonant excitation of the bubbles which have natural frequencies less than the excitation frequency contributes significantly to the amplitude of the fundamental harmonic and this is not strongly influenced by the reduction in the viscous and surface tension parameters for the ocean conditions. However, bubble dynamics play a stronger role in the generation of the second harmonic through harmonic cascading and thus an increase in the amplitude of the second harmonic (with reduced effect of viscosity and surface tension at the ocean conditions) may be expected. Hence, stronger harmonic cascading can be expected for the ocean conditions. An increase in the amplitude of wall oscillation was seen to simply increase the magnitude of the response without any changes in the features of the frequency response.

6. Limitations

In this section we shall examine the various limitations of the present model. The limitation imposed by the continuum mechanics model have been discussed in detail by d'Agostino & Brennen (1988) and so we focus here on additional considerations necessary in the present analysis.

First, the amplitude of the radius oscillation is required to be small; in particular, $|R_n/R_0| \ll 1$ must be satisfied. This is also implied in confining the solution to the oscillation of gas bubbles. Moreover, the effect of damping is also reduced for large bubbles. These restrictions place an upper limit on the excitation for the present analyses. In practice, $|R_n/R_0| \ll 1$ is expected to dictate the maximum applicable excitation for which the theory remains applicable.

The range of void fraction over which the present theory may be applied is also bounded on an upper and a lower limit. The lower limit of the void fraction is determined by the maximum bubble separation required under the continuum assumption as well as the requirement of maximum permissible amplitude of radius oscillation, $|R_n/R_0|$. The upper limit on void fraction is determined by the requirement

of local pressure disturbance to be negligible in comparison to the global pressure oscillation (d'Agostino & Brennen 1988).

The phenomenon of rectified diffusion results in slow growth of the equilibrium size of a bubble (Hsieh & Plesset 1961). Thus, the theory can be applied to bubbly layers subject to steady-state oscillation for long periods only if the equilibrium size, R_0 , is tracked and the values appropriate to a particular time are employed.

7. Some practical observations

Though limited to small-amplitude oscillations and thus to a small excitation, the qualitative phenomena uncovered here are valuable to bear in mind when interpreting some of the practical observations of the response of bubbly mixtures. In particular, harmonic cascading should be present in many practical situations. Measurements of spectra reported by Mellen (1954) and Blake (1986) appear to contain peaks which may be due to harmonic cascading. The results of Arakeri & Shanmuganathan (1985) do not exhibit harmonic cascading. However, that may be due to lack of variation in the size of bubbles generated by electrolysis. It may be important to keep this in mind while designing experiments for evaluating interactive effects in bubbly mixtures. It is particularly important to note that most of the spectra reported in the literature have been made using half-octave frequency resolution. Clearly, a finer spectral resolution in the spectra measurement is required in order to unambiguously resolve harmonic cascading.

8. Summary and conclusions

In this work we have studied some of the nonlinear effects which can occur when a plane wall bounding a bubbly liquid oscillates in a direction normal to itself. The principal results may be summarized as follows.

The presence of a finite lengthscale such as the finite thickness of the bubble layer results in characteristic natural frequencies of the bubble layer (known as cloud natural frequencies), all of which are less than the bubble natural frequency, ω_b . The natural frequencies are determined mainly by the void fraction and the ratio of thickness of the layer to the bubble radius. The dominant response occurs for excitation at the lowest cloud natural frequency and the response is dominated by the first- and second-harmonic components. Since the amplitude of the second harmonic is significant, not all of high-frequency response is damped out (in contrast to the results from linearized analysis). The amplitude of the response increases as the lowest natural frequency gets closer to about $0.5\omega_b$. The cloud natural frequencies become very small when the ratio of layer thickness to bubble radius becomes large and the resulting frequency response tends to that for a semi-infinite layer.

For excitation frequencies in the sub-resonant and trans-resonant regimes ($\omega < \omega_b$), the amplitude of oscillation forms standing wave patterns in the layer. The amplitude of these waves decays slowly with distance from the oscillating wall. However, for super-resonant excitation the oscillation amplitude decays rapidly with distance from the source of excitation (wall). This rapid decay is caused by the reduced role of bubble dynamics in the super-resonant regime in which the bubbly layer behaves like a homogeneous compressible fluid.

The phenomenon of harmonic cascading is seen to take place in a bubbly mixture containing bubbles of different sizes. Harmonic cascading occurs when a low-frequency excitation applied to the layer at a frequency ω_f results in a large amplitude

of oscillation at the frequency $2\omega_f$ due to the presence of a large number of bubbles with natural frequency of $2\omega_f$. The ratio of the amplitude of the second harmonic to the amplitude of the first harmonic defines the extent of harmonic cascading. This ratio increases with an increase in the number of bubbles with small radii relative to the number of bubbles with large radii. It is noteworthy that the phenomenon of harmonic cascading can only be modelled by a nonlinear model because the linearized models do not allow for such harmonic generation. In view of the results from this analysis, other kinds of links among timescales such as among subharmonics of different bubble sizes must be taken into account for strongly nonlinear solutions of bubble clouds.

Larger values of the void fraction cause a reduction in the amplitude of pressure and radius oscillation in all cases. This may imply reduced acoustic noise in the bubbly mixtures and damage potential in cavitating flows. The reduction of acoustic noise for larger void fraction has been observed experimentally by Arakeri & Shanmuganathan (1985). Furthermore, the larger number of bubbles present at large void fractions may cause stronger dissipation and a reduced amplitude of oscillation.

The authors are grateful for the support of Office of Naval Research under contract N000167-85-K-0165. The authors are also grateful to the reviewers for their helpful comments and suggestions included in the paper.

REFERENCES

- D'AGOSTINO, L. & BRENNEN, C. E. 1988 Linearized dynamics of spherical bubble clouds. *J. Fluid Mech.* **199**, 155–176.
- D'AGOSTINO, L., BRENNEN, C. E. & ACOSTA, A. J. 1988 Linearized dynamics of two-dimensional bubbly and cavitating flows over slender surfaces. *J. Fluid Mech.* **192**, 485–509.
- ARAKERI, V. H. & SHANMUGANATHAN, V. 1985 On the evidence for the effect of bubble interference on cavitation noise. *J. Fluid Mech.* **159**, 130–150.
- BIESHEUVEL, A. & WIJNGAARDEN, L. VAN 1984 Two phase flow equations for a dilute dispersions of gas bubbles in liquid. *J. Fluid Mech.* **148**, 41–52.
- BIRNIR, B. & SMEREKA, P. 1990 Existence theory and invariant manifolds of bubble clouds. *Commun. Pure Appl. Maths* **13**, 363–413.
- BLAKE, W. K. 1986 Propeller cavitation noise: the problems of scaling and prediction. *Intl Symp. on Cavity and Multiphase Flow Noise*, pp. 89–99.
- BLAKE, W. K., WOLPERT, M. J. & GEIB, F. E. 1977 Cavitation noise and inception as influenced by boundary layer development on a hydrofoil. *J. Fluid Mech.* **80**, 617–640.
- BRENNEN, C. E. & CECCIO, S. L. 1989 Recent observations on cavitation and cavitation noise. *Third Intl Symp. on Cavitation Noise and Erosion in Fluid Systems, San Francisco, CA, Dec. 1989*, pp. 67–78.
- CECCIO, S. L. & BRENNEN, C. E. 1991 The dynamics and acoustics of travelling bubble cavitation. *J. Fluid Mech.* **233**, 633–660.
- CHAHINE, G. L. 1982 Pressure field generate by the collective collapse of cavitation bubbles. *IAHR Symp. on Operating Problems of Pump Stations and Power Plants, Amsterdam, Netherlands*, Vol. 1 (2), pp. 1–12.
- CHAHINE, G. L. 1983 Cloud cavitation: theory. *14th Symp. on Naval Hydrodynamics*, pp. 165–195. National Academy Press.
- DEVIN, C. 1959 Survey of thermal, radiation and viscous damping of pulsating air bubbles in water. *J. Acoust. Soc. Am.* **31**, 1654–1667.
- ELLER, A. & FLYNN, H. G. 1969 Generation of subharmonics of order one-half by bubbles in sound field. *J. Acoust. Soc. Am.* **46**, 722–727.
- FLYNN, H. G. 1964 Physics of acoustics cavitation in liquids. In *Physical Acoustics – Principles and Methods* (ed. W. P. Mason), Vol. 1, Part B, pp. 57–172. Academic.

- GATES, E. M. & ACOSTA, A. J. 1978 Some effects of several free stream factors on cavitation inception on axisymmetric bodies. *12th Symp. on Naval Hydrodynamics, Washington, DC*, pp. 86–108.
- HANSSON, I., KEDRINSKII, V. & MØRCH, K. A. 1982 On the dynamics of cavity clusters. *J. Phys. D: Appl. Phys.* **15**, 1725–1734.
- HSIEH, D. Y. & PLESSET, M. S. 1961 Theory of rectified diffusion of mass into gas bubbles. *J. Acoust. Soc. Am.* **33**, 206–215.
- KUMAR, S. 1991 Some theoretical and experimental studies of cavitation noise. PhD thesis, Div. of Engng and Appl. Sci., Calif., Inst. of Tech.
- LAUTERBORN, W. 1976 Numerical investigation of nonlinear oscillations of gas bubbles in liquids. *J. Acoust. Soc. Am.* **59**, 283–293.
- MAEDA, M., YAMAGUCHI, H. & KATO, H. 1991 Laser holography measurement of bubble population in cavitation cloud on a foil section. *1st ASME/JSME Conf., Portland, Oregon, June 1991*, FED Vol. 116, pp. 67–75.
- MARBOE, M. L., BILLET, M. L. & THOMPSON, D. E. 1986 Some aspects of travelling bubble cavitation and noise. *Intl Symp. on Cavitation and Multiphase Flow Noise*, ASME, FED Vol. 45, pp. 119–126.
- MELLEN, R. H. 1954 Ultrasonic spectrum of cavitation noise in water. *J. Acoust. Soc. Am.* **26**, 356–360.
- MØRCH, K. A. 1980 On the collapse of cavity clusters in flow cavitation. In *Cavitation and Inhomogeneities in Underwater Acoustics* (ed. W. Lauterborn), pp. 95–100. Springer.
- MØRCH, K. A. 1982 Energy considerations in the collapse of cavity clusters. *Appl. Sci. Res.* **38**, 313–321.
- MØRCH, K. A. 1989 On cavity cluster formation in a focused acoustic field. *J. Fluid Mech.* **201**, 57–76.
- OMTA, R. 1987 Oscillations of a cloud of bubbles of small and not so small amplitude. *J. Acoust. Soc. Am.* **82**, 1018–1033.
- PARLITZ, U., ENGLISCH, V., SHEFFCZYK, C. & LAUTERBORN, W. 1990 Bifurcation structure of bubble oscillators. *J. Acoust. Soc. Am.* **88**, 1061–1077.
- PLESSET, M. S. & HSIEH, D. Y. 1960 Theory of gas bubble dynamics in oscillating pressure fields. *Phys. Fluids* **3**, 882–892.
- PLESSET, M. S. & PROSPERETTI, A. 1977 Bubble dynamics and cavitation. *Ann. Rev. Fluid Mech.* **9**, 145–185.
- PROSPERETTI, A. 1974 Nonlinear oscillations of gas bubbles in liquids: steady state solutions. *J. Acoust. Soc. Am.* **56**, 878–885.
- PROSPERETTI, A. 1975 Nonlinear oscillations of gas bubbles in liquids: transient solutions and the connection between subharmonic signal and cavitation. *J. Acoust. Soc. Am.* **57**, 878–885.
- PROSPERETTI, A. 1977 Application on subharmonic threshold to the measurement of the damping of oscillating gas bubbles in liquids. *J. Acoust. Soc. Am.* **61**, 17–27.
- TANGREN, R. F., DODGE, C. H. & SEIFERT, H. S. 1949 Compressibility effects in two-phase flows. *J. Appl. Phys.* **20**, 637–645.
- VAUGHN, P. W. 1968 Investigation of acoustic cavitation thresholds by observation of the first subharmonic. *J. Sound. Vib.* **7**, 236–246.
- WIJNGAARDEN, L. VAN 1964 On the collective collapse of large number of gas bubbles in water. *Proc. of 11th Intl Cong. of Appl. Mech.*, pp. 854–861. Springer.